

St. Cloud State University

## The Repository at St. Cloud State

---

Culminating Projects in Electrical Engineering

Department of Electrical and Computer  
Engineering

---

12-2022

### Testing of a ZedBoard-Based System for EIT Image Reconstruction

Robert DuBois

Follow this and additional works at: [https://repository.stcloudstate.edu/ece\\_etds](https://repository.stcloudstate.edu/ece_etds)

---

#### Recommended Citation

DuBois, Robert, "Testing of a ZedBoard-Based System for EIT Image Reconstruction" (2022). *Culminating Projects in Electrical Engineering*. 9.

[https://repository.stcloudstate.edu/ece\\_etds/9](https://repository.stcloudstate.edu/ece_etds/9)

This Thesis is brought to you for free and open access by the Department of Electrical and Computer Engineering at The Repository at St. Cloud State. It has been accepted for inclusion in Culminating Projects in Electrical Engineering by an authorized administrator of The Repository at St. Cloud State. For more information, please contact [tdsteman@stcloudstate.edu](mailto:tdsteman@stcloudstate.edu).

# **Testing of a ZedBoard-Based System for EIT Image Reconstruction**

by

Robert DuBois

A Thesis

Submitted to the Graduate Faculty of

St. Cloud State University

in Partial Fulfillment of the Requirements

for the Degree of

Master of Science

December, 2022

Thesis Committee:  
Yi Zheng, Chairperson  
Ling Hou  
Michael Glazos

### **Abstract**

Improvements in Electrical Impedance Tomography (EIT) are discussed: first, the extension of our current real-time EIT system to allow for multiple shapes by post-hoc estimation of the image, then the prospect of taking images of a static material, but with the homogeneous and inhomogeneous data taken at two different frequencies. Images with various shapes are produced and shown; the impracticality of using multiple frequency imaging with the current EIT system is also shown. Multiple frequency images are produced with a different, non-real-time system. In addition, the procedure for producing the phantom test material is discussed.

### **Acknowledgements**

Credit goes to Yi Zheng for proposing using frequency dispersion for EIT imaging, to Gegg for making the cross-frequency EIT image in chapter 8, and to Monali for designing the base software used for our EIT images.

**Table of Contents**

	Page
List of Tables .....	6
List of Figures .....	7
Chapter	
1. Introduction.....	9
2. EIT Basics.....	10
2.1 EIT Overview .....	10
2.2 Medical Imaging .....	10
2.3 General EIT System Design .....	10
2.4 Forward and Inverse Problems.....	11
2.5 Mathematical Forward Problem.....	11
2.6 The Inverse Problem .....	12
3. Finite Element Method .....	14
3.1 FEM Overview .....	14
3.2 FEM Math .....	14
4. Previous Work .....	17
4.1 Previous Project Overview .....	17
4.2 Board Design Specifications .....	17
4.3 Board Hardware Design .....	20
4.4 Board Software/Previous EIT .....	24
4.5 Initial Board Results.....	32

Chapter	Page
5. Phantom Design .....	34
5.1 Phantom Overview .....	34
5.2 Phantom Procedure .....	34
6. Proposed Work.....	36
6.1 Overview .....	36
6.2 Non-circular Phantoms.....	36
6.3 Frequency Dispersion and Cross-frequency Imaging .....	36
7. Arbitrary Shape Results .....	38
7.1 Arbitrary Shape Modifications.....	38
7.2 Arbitrary Shape Algorithm .....	38
7.3 Arbitrary Shape Results .....	39
8. EIT using Different Frequencies.....	43
8.1 Tissue Impedance Dispersion.....	44
8.2 EIT Image using Two Different Frequencies for Changed Tissue Phantom .....	46
8.3 Differing Frequency Images.....	47
9. Analysis.....	50
9.1 Arbitrary Shape Analysis .....	50
9.2 Multiple Frequency Analysis .....	50
10. Conclusion .....	52
Works Cited .....	53

**List of Tables**

Table	Page
4.1. Text controls .....	31
5.1. Phantom composition.....	34

## List of Figures

Figure	Page
3.1. The mesh used for EIT calculations.....	14
4.1. Image of the board .....	17
4.2. IEC AC safety graph.....	19
4.3. System flowchart .....	20
4.4. DAC, on evaluation board .....	21
4.5. AD7761, on evaluation board and ZedBoard .....	22
4.6. PCB diagram.....	22
4.7. Switching system schematic .....	23
4.8. Software block diagram .....	25
4.9. EIT reconstruction block diagram .....	26
4.10. PL block diagram.....	27
4.11. DAC and switching control .....	27
4.12. Receiving block diagram .....	28
4.13. DFT code .....	30
4.14. GUI screenshot.....	31
4.15. Phantom image, homogenous data. For inhomogenous data, the left hole was filled and the bottom one was emptied. ....	32
4.16. Output image, taken with 8192 samples at 10 kHz .....	33
7.1. A circular mesh and its corresponding elliptical mesh .....	38
7.2. Elliptical phantom.....	39



Figure	Page
7.3. Elliptical results .....	40
7.4. Triangular phantom.....	40
7.5. Triangular results .....	41
7.6. Off-center circular phantom. Electrode 1 is the brown one at the top left.....	41
7.7. Off-center circular image. Image was originally mirrored due to the electrodes being put on counterclockwise, but was corrected. ....	42
8.1. Transmission coefficients of tissue phantom.....	45
8.2. Transmission coefficients of tissue phantom with brain tissue .....	45
8.3. Ratios of transmission coefficients of phantom and phantom with lamb brain.....	46
8.4. Lamb brain tissue embedded in a tissue phantom .....	48
8.5. EIT image of lamb brain tissue using 500 Hz and 199 kHz. ....	49

## **Chapter 1: Introduction**

Previous groups at this university have designed and developed a system for using EIT to capture images of phantom but did not rigorously test the product of their research. This thesis aims to change this by testing the system across the range of its capabilities. This thesis is in two parts; in the first, a modification to the system to allow for arbitrary input shapes is proposed and implemented. In the second, modifications to allow for cross frequency imaging are discussed.

In this document, first, the thesis is introduced, then, an overview of EIT is provided. Afterwards, it covers the finite element method, the specific implementation of the system, and the design and composition of the test phantoms. Finally, the proposed work is discussed.

## Chapter 2: EIT Basics

### 2.1 EIT Overview

EIT (electrical impedance tomography) is an imaging method that uses electrodes at the surface of an object to generate a map of its impedance. The imaging is accomplished by injecting an AC current into electrodes in sequence, then feeding the data from the other electrodes into a computer of some sort to do reconstruction. Most EIT systems use a difference method to compute their images; they show how the impedance has changed from a reference image. This is known as time-difference EIT. While absolute EIT (EIT without a reference image) is possible, it is outside the scope of this paper, and further discussion will be focused on time-difference EIT. The image produced is split into triangles for the finite element method.

### 2.2 Medical Imaging

The main application for EIT is as a medical imaging technique. Generally, it can be used when an area of conductive material changes its conductivity without changing its shape. This leads to many medical applications, such as imaging the lungs to monitor airflow or monitoring the brain for hemorrhages. Compared to other medical imaging, EIT has the advantages of portability and speed, but produces comparatively low-resolution images.

### 2.3 General EIT System Design

Necessary parts of any EIT system include the control unit, electrode ring, current source, and ADC. The control unit turns on the current source, which provides current to the electrode ring around the area of interest, which sends signals back to the ADC, which is read by the control unit. Then, the data recovered is processed and used to make an image.

In the system discussed in this paper, the electrode ring is 12 elements, and current is injected into the target area from opposite sides, known as T+ and T-. In order to generate the

complete data used for reconstruction, T+ and T- rotate to each of the 12 electrodes when taking an image.

## 2.4 Forward and Inverse Problems

In the EIT algorithm, solving for the impedance distribution from the known voltage measurements and injected current is known as the inverse problem. In order to find a solution to the inverse problem, it is necessary to also solve the forward problem – solving for the voltage distribution from the calculated impedance distribution and the injected current. Solving the forward problem allows for an iterative approach to the inverse problem. In the system covered in this paper, the forward problem is solved using the finite element method.

## 2.5 Mathematical Forward Problem

Mathematically, the equations governing the forward problem can be derived from Maxwell's equations; first, take:

$$\nabla \cdot \mathbf{E} = \frac{\rho}{\epsilon_0}$$

(Gauss's law)

EIT systems, generally, can have frequencies of up to 50 kHz. However, the system discussed in this paper has a maximum frequency of 10 kHz. As the injected current is up to 10 kHz and the target area is approximately .3 meters wide. The relative permittivity of grey matter at 10 kHz is 3000, so the wavelength is approximately 500 meters at 10 kHz, which is much larger (using the 1% guideline for “much larger”) than the size of the phantom (Gabriel, et al. 2238).

For a phantom with no internal current sources, assuming the phantom is much smaller than the wavelength of the injected current, the field can be approximated by a divergence-free, near-static field, so:

$$\nabla \cdot \mathbf{E} = 0$$

(Gauss's law for divergence-free fields)

and

$$\mathbf{E} = -\nabla V$$

(relation between E and V for static fields)

Putting together the last two equations makes the equation used to solve the EIT forward problem:

$$\nabla^2 V = 0$$

(by substitution)

## 2.6 The Inverse Problem

In order to solve the inverse problem, first, we define the Jacobian matrix,  $\mathbf{J}$ , as a [number of elements in the finite element method mesh] by [number of measurements] matrix that, when multiplied by the vector formed by the conductivity change of each element (represented by  $\mathbf{x}$ ), produces the measurements (represented by  $\mathbf{y}$ ), plus noise (represented by  $\mathbf{n}$ , and generally ignored in later calculations). This equation is:

$$\mathbf{y} = \mathbf{J}\mathbf{x} + \mathbf{n}$$

$\mathbf{J}$  can be determined through application of the finite element method to the forward problem; this is discussed in the next section. As  $\mathbf{J}$  is not an invertible matrix, this equation cannot be solved directly; rather, the solution must be approximated by minimizing the least-square error:

find  $\mathbf{x}$  such that  $\|\mathbf{y} - \mathbf{J}\mathbf{x}\|^2$  is minimized

Generally, there are multiple solutions to this problem, so additional constraints, known as regularization, must be used to get the desired solution. To regularize the problem, an additional term is added:

$$\text{find } \mathbf{x} \text{ such that } \|\mathbf{y} - \mathbf{J}\mathbf{x}\|^2 + \lambda^2 \mathbf{z} \text{ is minimized}$$

where  $\mathbf{z}$  is the length of the vector formed by multiplying the regularization matrix and  $\mathbf{x}$ .

Assuming no variation in measurement quality between channels, the solution to this equation is approximated by taking

$$\mathbf{x} = (\mathbf{J}^T \mathbf{J} + \lambda^2 \mathbf{R})^{-1} \mathbf{J}^T \mathbf{y}$$

where  $\mathbf{R}$  is the regularization matrix and  $\lambda$  is the regularization hyperparameter, which is the average amplitude of the noise divided by the average amplitude of the signal, which is generally approximated. When using the Tikhonov prior, like in the system in this paper, the regularization matrix is the identity matrix  $\mathbf{I}$ .

This equation is unconstrained; solving it requires a boundary condition to be applied. As the system discussed in this paper uses the Neumann boundary for its calculations, it will be the only type discussed. The Neumann boundary for EIT states that, for normal vector to the boundary  $\mathbf{n}$  and surface current  $I$  on the surface  $S$ :

$$\sigma \frac{\partial V}{\partial \mathbf{n}} = I \text{ at } S$$

and

$$\int_S I ds = 0$$

This is useful when using the finite element method to generate an EIT image, discussed in the next section.

## Chapter 3: Finite Element Method

### 3.1 FEM Overview

In the finite element method, a space is broken up into discrete elements so that a system of equations representing the space can be formed by analyzing the individual elements. The results of this are an approximation of the state of the system. More specifically, for this system, the area of the phantom is broken up into a triangular mesh, the current and impedance are treated as given, and the voltage is solved for. See Figure 3.1 for an image of this mesh.

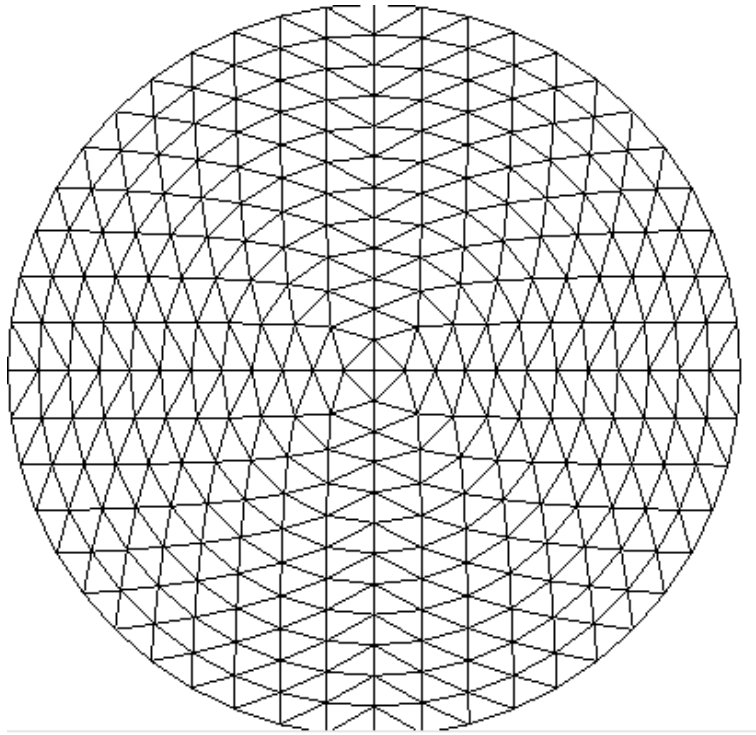


Figure 3.1. The mesh used for EIT calculations

### 3.2 FEM Math

For any individual element, the potential is approximated linearly in two dimensions, so it is:

$$V_e(x, y) = ax + by + c$$

The three corner nodes are assumed to be equal across elements, so we calculate  $V_{e1}$ ,  $V_{e2}$ , and  $V_{e3}$  to be those voltages (reading clockwise around the triangle):

$$\begin{bmatrix} V_{e1} \\ V_{e2} \\ V_{e3} \end{bmatrix} = \begin{bmatrix} x_1 & y_1 & 1 \\ x_2 & y_2 & 1 \\ x_3 & y_3 & 1 \end{bmatrix} * \begin{bmatrix} a \\ b \\ c \end{bmatrix}$$

$V_e$  can be restated like this:

$$V_e(x, y) = \begin{bmatrix} a \\ b \\ c \end{bmatrix} \cdot \begin{bmatrix} x \\ y \\ 1 \end{bmatrix}$$

So, to substitute out a, b, and c in  $V_e$ :

$$\begin{bmatrix} a \\ b \\ c \end{bmatrix} = \begin{bmatrix} x_1 & y_1 & 1 \\ x_2 & y_2 & 1 \\ x_3 & y_3 & 1 \end{bmatrix}^{-1} * \begin{bmatrix} V_{e1} \\ V_{e2} \\ V_{e3} \end{bmatrix}$$

Calculating out the inverse, we get:

$$\begin{bmatrix} a \\ b \\ c \end{bmatrix} = \frac{1}{\begin{vmatrix} x_1 & y_1 & 1 \\ x_2 & y_2 & 1 \\ x_3 & y_3 & 1 \end{vmatrix}} \begin{bmatrix} y_2 - y_3 & y_3 - y_1 & y_1 - y_2 \\ x_3 - x_2 & x_1 - x_3 & x_1 - x_2 \\ x_2 y_3 - x_3 y_2 & x_3 y_1 - x_1 y_3 & x_1 y_2 - x_2 y_1 \end{bmatrix} * \begin{bmatrix} V_{e1} \\ V_{e2} \\ V_{e3} \end{bmatrix}$$

The determinant on bottom of the fraction is equal to plus or minus the area of the element. It is positive if and only if the nodes are numbered clockwise and will be assumed to be positive for further calculations.

Substituting back in to  $V_e$  produces:

$$V_e(x, y) = \left( \frac{1}{2A} \begin{bmatrix} y_2 - y_3 & y_3 - y_1 & y_1 - y_2 \\ x_3 - x_2 & x_1 - x_3 & x_1 - x_2 \\ x_2 y_3 - x_3 y_2 & x_3 y_1 - x_1 y_3 & x_1 y_2 - x_2 y_1 \end{bmatrix} * \begin{bmatrix} V_{e1} \\ V_{e2} \\ V_{e3} \end{bmatrix} \right) \cdot \begin{bmatrix} x \\ y \\ 1 \end{bmatrix}$$

These are the equations used to approximate one element of the mesh. Next, we use the method of weighted residuals. For each element, we set the integral over the element of the weight  $W$  times the residual to be zero. The residual  $R$  is the error in  $\nabla^2 V$  between the FEM approximation and zero. This gives the equation:



$$\int_A W \nabla^2 V \, dA = 0$$

or

$$\int_A W \nabla \cdot \sigma \nabla V \, dA = 0$$

where  $\sigma$  is the conductivity of the element. Putting this in terms of a line integral gives:

$$\int_L W \sigma \nabla V \, dL = 0$$

Next, define an  $i$  by  $j$  stiffness matrix  $A$  as follows: (Polydorides, 13-37)

$$A_{i,j} = \int_A \sigma \nabla W_i \cdot \nabla W_j \, dA$$

where  $W_i$  in our case is  $V_{e1}$ , and  $i$  and  $j$  run from 1 to the number of vertices of the element.

We also need matrix  $B$  and vector  $C$  for an element on the boundary:

$$B_{i,j} = \int_L \frac{W_i \cdot W_j}{z_l} \, dL$$

$$C_i = \int_L -\frac{W_i}{z_l} \, dL$$

$z_l$  is the electrode impedance. From above, these matrices follow the equation:

$$(A + B)V_i = CV_i$$

where  $V_1$  is the voltage at the boundary electrode nodes and  $V_i$  is the voltage at a mesh point.

Ignoring power dissipation at the surface of the phantom, these equations can then be solved for

$V$ .

## Chapter 4: Previous Work

### 4.1 Previous Project Overview

In Spring 2018, a group of undergraduate students, Christopher Burg, Robert DuBois, Laura Hengel, and Joseph Kelzenberg, designed the board this thesis' work is based on. The board was a PCB attached to a ZedBoard through the FMC LPC port, which sent data to a computer via a mini USB to USB cable. In general terms, it took circular EIT images at single frequencies, then used the computer to finish calculations and display the image. As this board is being used as a basis for this thesis, details of it will be discussed.

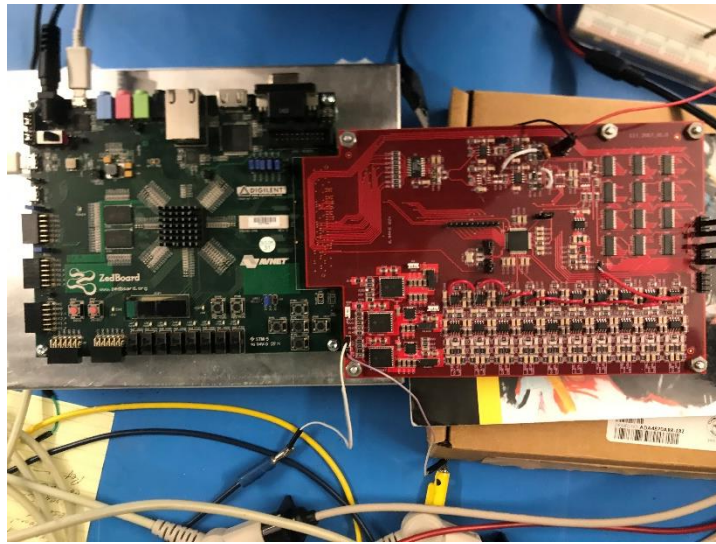


Figure 4.1. Image of the board

### 4.2 Board Design Specifications

These were the original specifications used when designing the board:

- Digital data of sinusoidal signals or pulses with a selected amplitude and frequency are generated by a DDS implemented within the Zynq chip.
- DAC (16 bits) converts the digital data of 16 bits to analog differential signals from 100 Hz to 100kHz.
- The differential signal will be conditioned by an analog front end (AFE) circuit.

- The conditioned signal will be converted to current by differential currents that are controllable from 0.1 to 1 mA RMS.
- The differential currents will be transmitted to two of the twelve electrodes through a switch system controlled by the Zynq chip.
- Eight adjacent voltage differences will be detected by using a total of ten electrodes.
- The eight received signals will be conditioned by a receiving circuit and be digitized by an eight-channel ADC (16 bits) afterwards it will be received by a Zynq SoC.
- The Zynq will demodulate the RF signal using FFT and process the data for EIT reconstruction.
- The Zynq will process the output of the FFT using EIT algorithms to obtain EIT images.
- The resolution of the EIT is determined by the memory size of the ZedBoard in the first stage and the DDR of the final system.
- Linux will run on the Zynq chip and will enable the display of the EIT image via the HDMI port.
- ZedBoard will be able to communicate with a PC for data storage, additional EIT processing, and the image display.
- A C# GUI will run on a PC which can also control the operation on the Zynq chip.

In addition, there were the following constraints:

- The current flow from the device must be kept at a safe level. The project ended up using a 1 mA current source, which is in the AC-2 zone of the IEC graph, meaning the current is detectable, can cause weak muscle contractions, and causes no permanent damage.

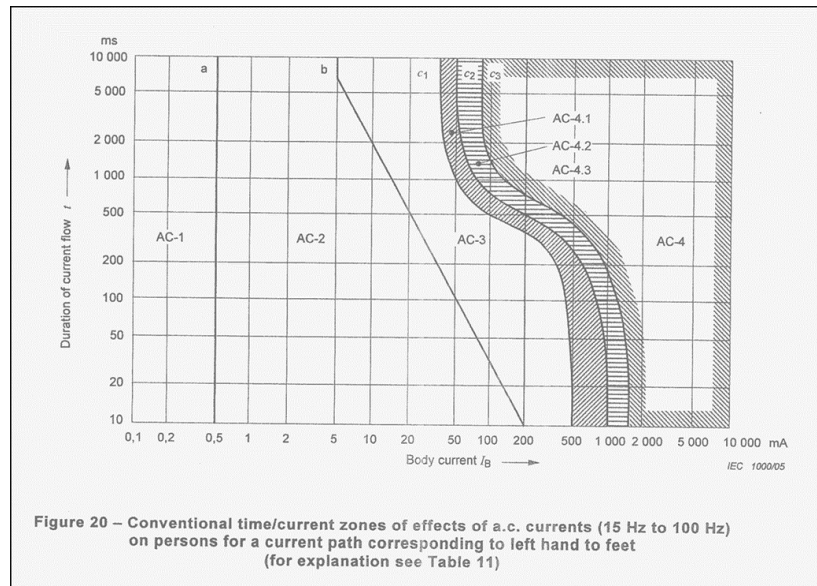


Figure 20 – Conventional time/current zones of effects of a.c. currents (15 Hz to 100 Hz) on persons for a current path corresponding to left hand to feet (for explanation see Table 11)

Table 11 – Time/current zones for a.c. 15 Hz to 100 Hz for hand to feet pathway – Summary of zones of Figure 20

Zones	Boundaries	Physiological effects
AC-1	Up to 0,5 mA curve a	Perception possible but usually no 'startled' reaction
AC-2	0,5 mA up to curve b	Perception and involuntary muscular contractions likely but usually no harmful electrical physiological effects
AC-3	Curve b and above	Strong involuntary muscular contractions. Difficulty in breathing. Reversible disturbances of heart function. Immobilization may occur. Effects increasing with current magnitude. Usually no organic damage to be expected
AC-4 <sup>1)</sup>	Above curve c <sub>1</sub>  c <sub>1</sub> -c <sub>2</sub>  c <sub>2</sub> -c <sub>3</sub>  Beyond curve c <sub>3</sub>	Patho-physiological effects may occur such as cardiac arrest, breathing arrest, and burns or other cellular damage. Probability of ventricular fibrillation increasing with current magnitude and time  AC-4.1 Probability of ventricular fibrillation increasing up to about 5 %  AC-4.2 Probability of ventricular fibrillation up to about 50 %  AC-4.3 Probability of ventricular fibrillation above 50 %

<sup>1)</sup> For durations of current flow below 200 ms, ventricular fibrillation is only initiated within the vulnerable period if the relevant thresholds are surpassed. As regards ventricular fibrillation, this figure relates to the effects of current which flows in the path left hand to feet. For other current paths, the heart current factor has to be considered.

Figure 4.2. IEC AC safety graph

- The system must be portable. In the project, this was defined loosely, but the system could easily be moved by hand, and more easily moved than an MRI, which was used as the benchmark for this.
- The system must be inexpensive, again compared to an MRI. The final system ended up costing around \$1300 to make.

### 4.3 Board Hardware Design

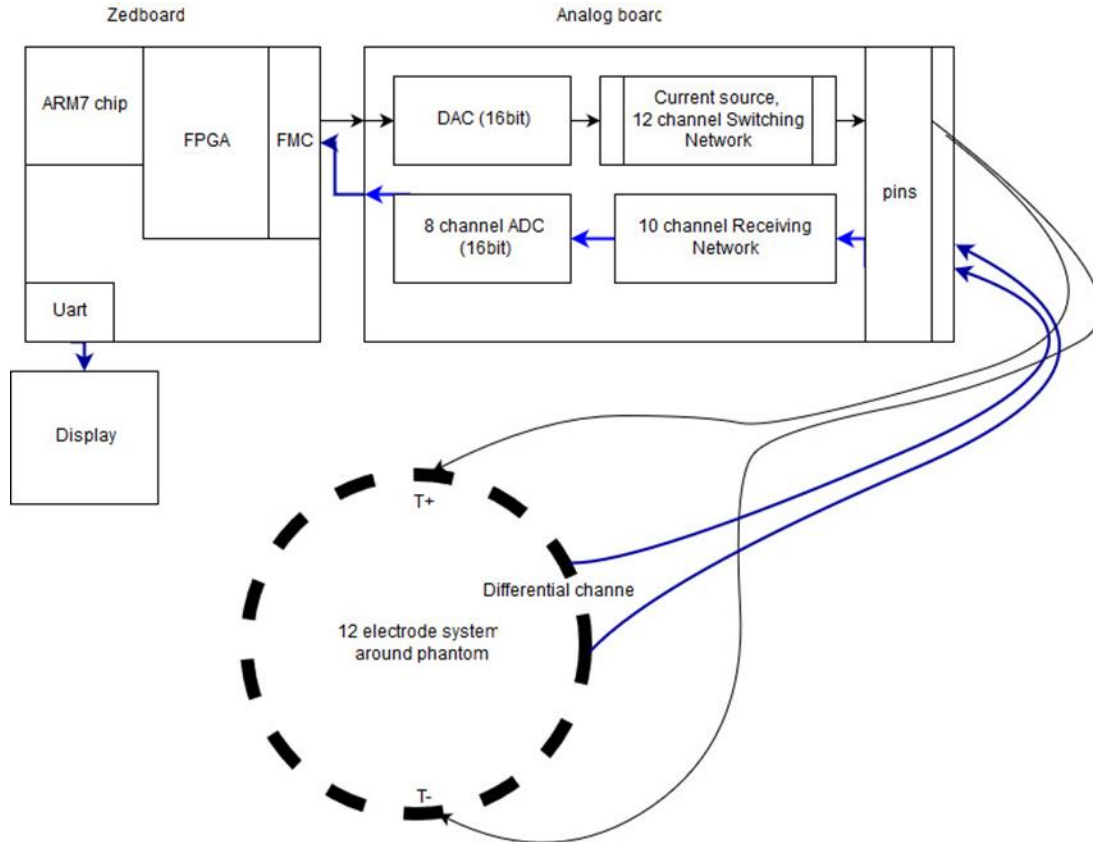


Figure 4.3. System flowchart

The PCB has several components, in order by when the signal passes through them:

An FMC LPC connector used to interface with the ZedBoard. This is essentially just a bank of digital I/O pins.

The LPC1668 DAC used to synthesize the 10 mA rms sinusoidal current injected into the phantom.



Figure 4.4. DAC, on evaluation board

From the transmitter, the current is injected into one of twelve electrodes placed evenly around a phantom. The current is injected into opposite electrodes, and data is received from the eight pairs of adjacent non-transmitting electrodes. For a full set of data, all twelve transmitter positions are used, for 96 total pieces of data. For a full image, two sets of data, one homogenous and one inhomogenous are taken, and the difference is found.

The AD7761 ADC. This is a 16 bit, 8 channel ADC used to receive all 8 relevant data channels from the phantom simultaneously. From here, the data is sent back through the FMC to the Zynq chip.



Figure 4.5. AD7761, on evaluation board and ZedBoard

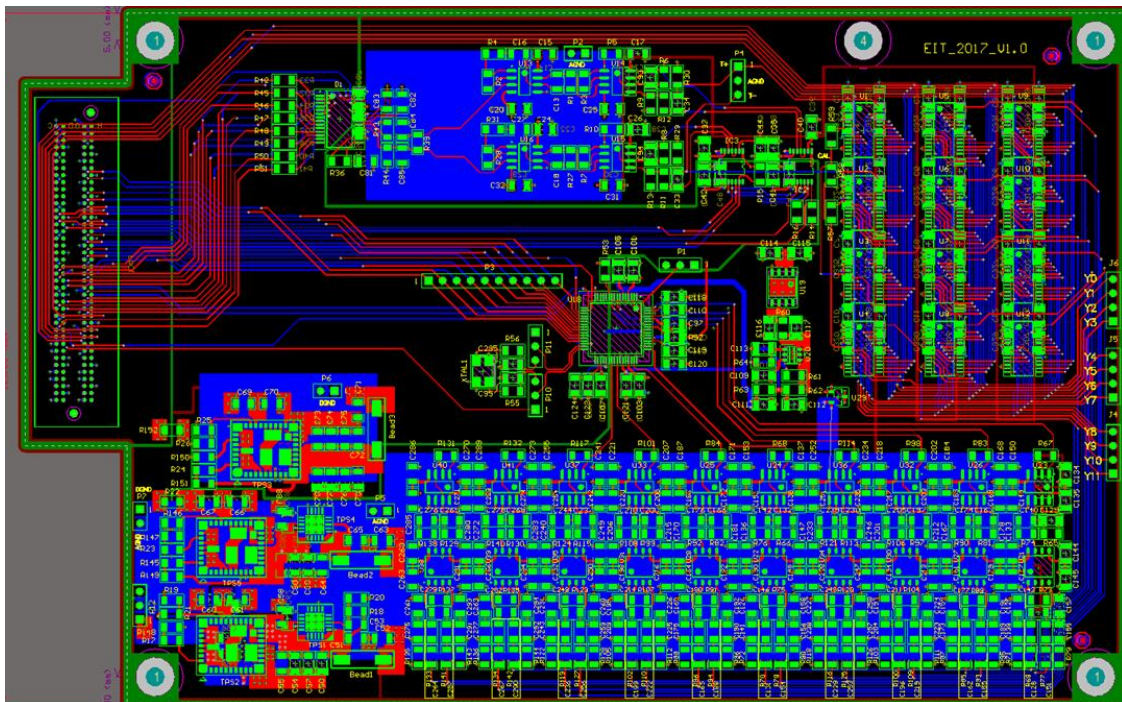


Figure 4.6. PCB diagram

This is the PCB used in the project. At the top is the transmitter, to the right is switching, the center is the ADC, the bottom is receiving, and power is in the lower left. Control and data from the ZedBoard are both passed in from the FMC at the left.

For the transmitter on the board, Signal\_T+ and Signal\_T- are the outputs from the DAC, used to control a current source that outputs to the switching system via T+ and T-. I am prohibited from providing the schematic of the transmitter here due to the original work being for a corporate project.

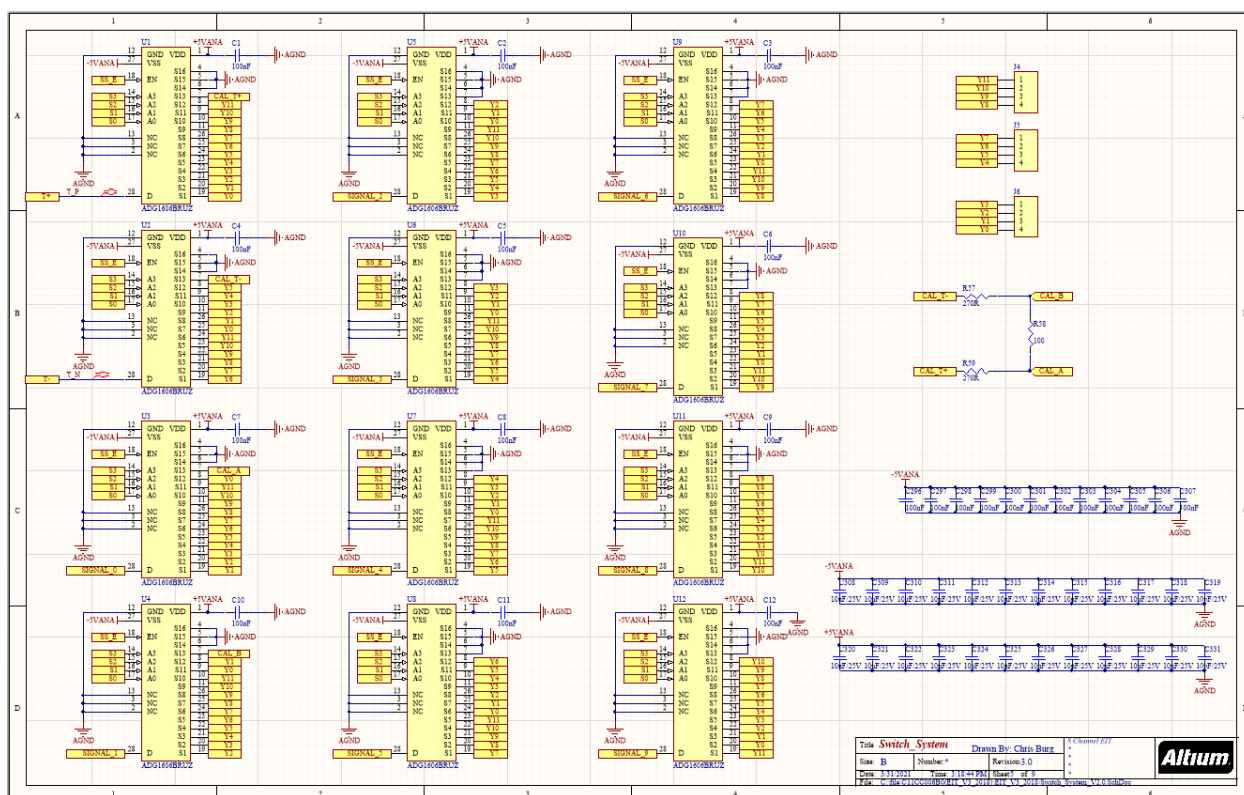


Figure 4.7. Switching system schematic

This is the board's switching system. Control lines S0 through S3 are used to select which position the transmitter is in. It is assumed that T+ and T- are on opposite sides of the phantom, and that the data is being collected from the eight pairs of adjacent electrodes that exist



when this is done. Note that the two pairs of electrodes going across the transmitter still are connected to a receiver, but not to the ADC.

Each receiving channel has a bandpass filter before going through an AD8429 instrumentation amplifier, then another bandpass filter and level shifter. The output of this goes to the ADC. I am prohibited from providing the schematic of the receiver here due to the original work being for a corporate project.

#### **4.4 Board Software/Previous EIT**

The software for running the board is divided into three main parts:

The programmable logic (PL) on the ZedBoard, used for interfacing with the hardware, calculating the product of the data and the Jacobian matrix, and storing the data from the ADC in FIFOs.

The processing system (PS) on the ZedBoard, used as a control unit for the PL, to calculate the discrete Fourier transform of the data, and to prepare data for transmitting to the GUI.

The graphical user interface (GUI) on the attached computer, used to make final calculations and adjustments for the data, to display the data, and to let the user input parameters for the EIT.

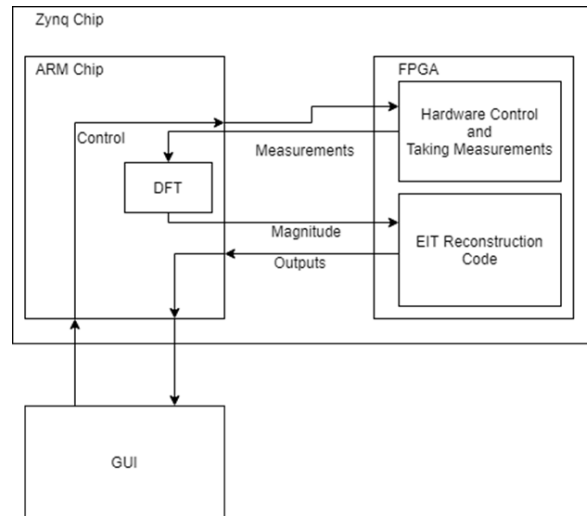


Figure 4.8. Software block diagram

Once the data from the phantom is received, the discrete Fourier transform of the data at the transmitted frequency is found. If homogenous data is being taken, these values are stored. Otherwise, the inhomogenous and homogenous data are then sent to the EIT reconstruction block (in the ZedBoard PL), where they are multiplied by the Jacobian matrix. Note that, due to hardware limitations encountered during the project, the Jacobian used in reconstruction is fixed to be for a structure made of 12 rings of triangles. Once the multiplication is done, the output values are sent back to the PS, which then sends them to the GUI for image construction and display. The hyperparameter for the system is constant. The project can handle frequencies in the range from 500 Hz to 10 kHz and can take a number of samples between 512 and 8192. These values are chosen by the user via the GUI.

This is the block diagram for the EIT reconstruction module. `Homo_mag` and `inhomo_mag` are registers used to store the input data to the block. When the enable signal is active, the difference in the magnitudes is taken by the `gen_dif_vector` modules, then the resulting vector is stored in the `differences` register. `RM` is a memory used to store the fixed Jacobian, which is accessed one column at a time by varying `another_index`. The

one\_dot\_product modules each take a single column of the reconstruction matrix and the difference vector and output the dot product of the two from the EIT reconstruction block. All signals sent to and by this block go back to the PS.

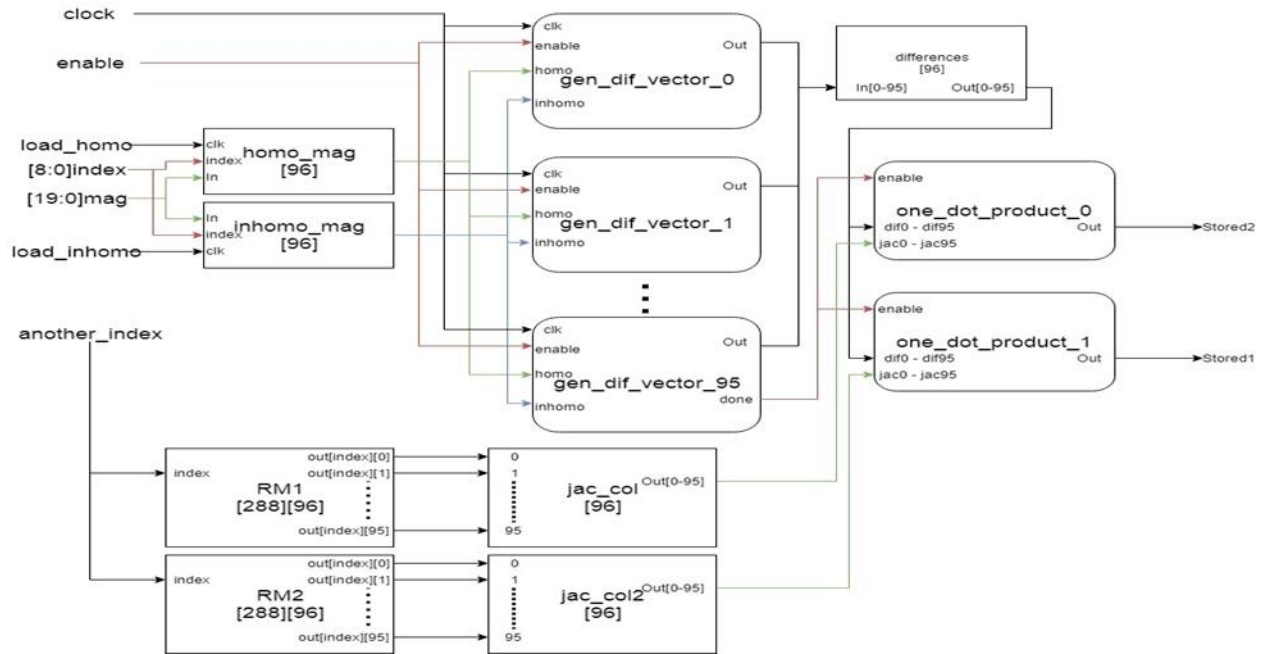


Figure 4.9. EIT reconstruction block diagram

This is the overall block diagram for the PL. This will be discussed section by section.

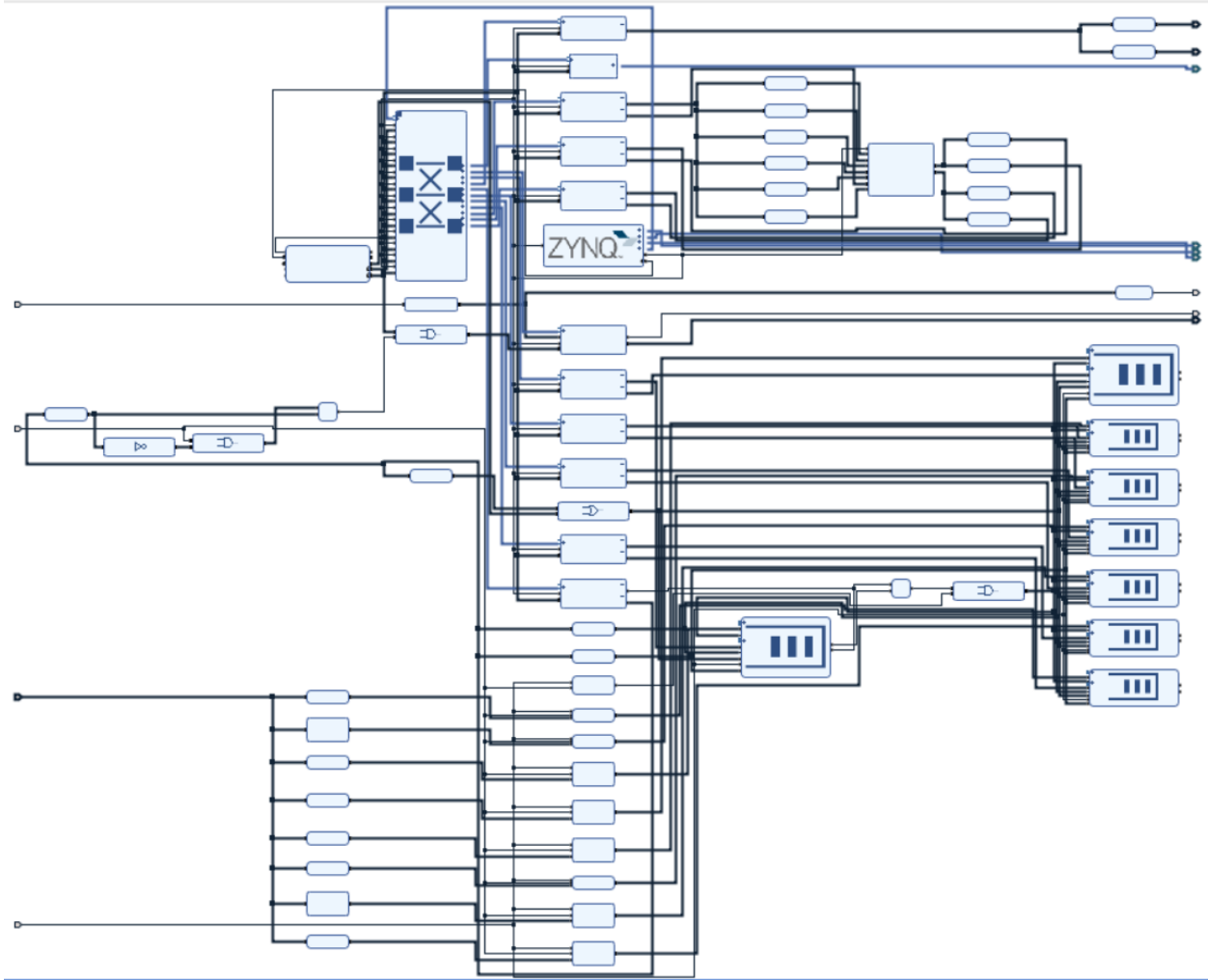


Figure 4.10. PL block diagram

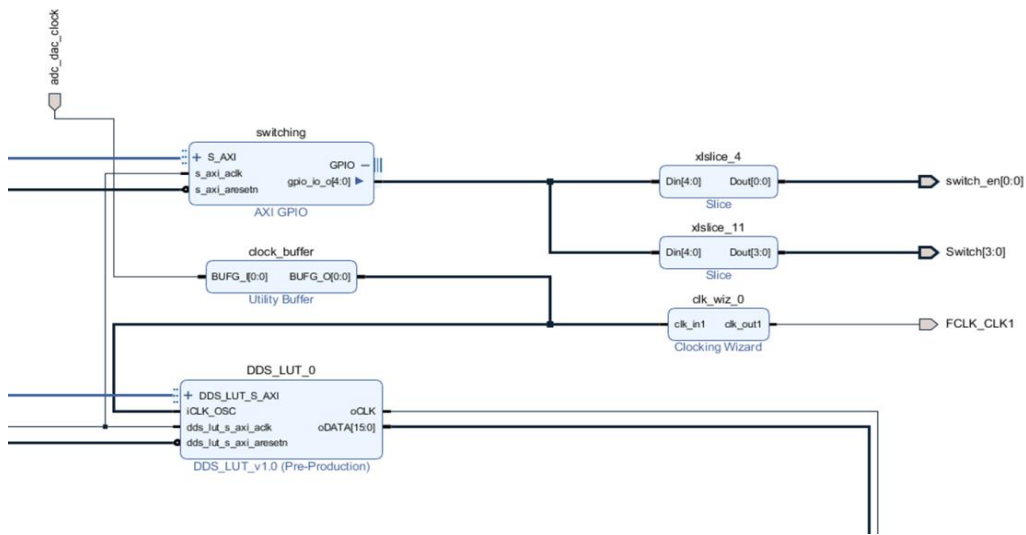


Figure 4.11. DAC and switching control

This is the section of the PL used to control the DAC and switching system. The DDS\_LUT block is a DAC controller that has 50,000 samples of a sine wave stored in it. It runs at a clock speed of 50 MHz by default. The DAC can be set to skip samples or to slow the clock to adjust the output frequency. The rest of this section is used for switching which electrodes the transmitter is connected to, via GPIO from the PS.

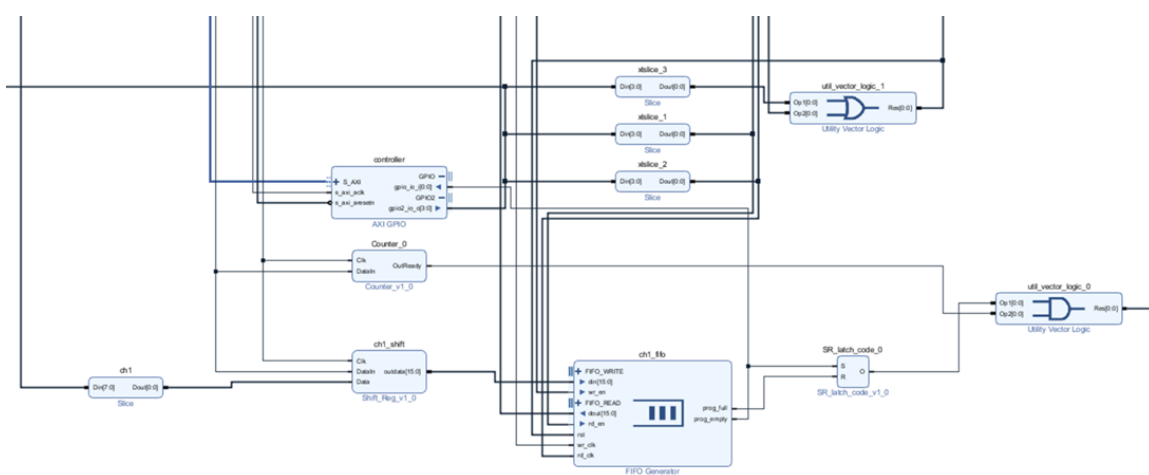


Figure 4.12. Receiving block diagram

This diagram shows the system for storing returning data from one channel of the ADC. There are eight of these, one for each channel. The incoming data is stripped of its 8-bit header, then stored in the FIFO. When a full set of samples was in the FIFO, the set was read into the PS for DFT calculations.

The ADC is controlled through SPI output through MIO on the PS. The code for this is below:

```
unsigned long* a = 0xE000A288;
*a = 0xFC0000;
a = 0xE000A284;
*a = 0xFC0000;
a = 0xE000A048;
*a = 0x440000;
```

```
SPI_send(0x0108);
SPI_send(0x0108);
```

This code first enables the GPIO bank used for MIO by setting the bytes at E000A288, E000A284, and E000A048, then uses the function `SPI_send` to set the ADC's power usage and sample rate.

```
void SPI_send(int data_in)
{
    int i = 15;
    int j = 0;
    unsigned long* a = (unsigned long*)0xE000A048;
    *a = 0x040000;
    while (j < 50) j++;
    while (i >= 0)
    {
        *a = 0x840000 + (((data_in >> i)%2)<<20);
        j = 0;
        while (j < 50) j++;
        *a = 0x040000 + (((data_in >> i)%2)<<20);
        i--;
        j = 0;
        while (j < 50) j++;
    }
    *a = 0x440000;
    j = 0;
    while (j < 50) j++;
    *a = 0xC40000;
    j = 0;
    while (j < 50) j++;
    *a = 0x440000;
    j = 0;
    while (j < 50) j++;
}
```

`SPI_send` is a software-side implementation of SPI, using `j` for a clock. The top six bits of `a` are connected to the SPI interface on the ADC. Bits are read in one at a time, starting at the most significant bit of `data_in`.

```

}
for(int counter = 0; counter < N; counter++)
{
    XGpio_DiscreteWrite(&controller, 2, 0x1);
    for(int i = 0; i < 300; i++){;}
    XGpio_DiscreteWrite(&controller, 2, 0x3);
    for(int i = 0; i < 300; i++){;}

    if(XGpio_DiscreteRead(&controller,1) != 1)
    {

        value[0] = XGpio_DiscreteRead(&ch1_2,1)-15000;
        value[1] = XGpio_DiscreteRead(&ch1_2,2)-15000;
        value[2] = XGpio_DiscreteRead(&ch3_4,1)-15000;
        value[3] = XGpio_DiscreteRead(&ch3_4,2)-15000;
        value[4] = XGpio_DiscreteRead(&ch5_6,1)-15000;
        value[5] = XGpio_DiscreteRead(&ch5_6,2)-15000;
        value[6] = XGpio_DiscreteRead(&ch7_8,1)-15000;
        value[7] = XGpio_DiscreteRead(&ch7_8,2)-15000;

        for(int i = 0; i < 8; i++)
        {
            accum[i] += value[i] * cos(counter * s[jstar][sstar] * PI2 / N)/1000;
            imag[i] += value[i] * sin(counter * s[jstar][sstar] * PI2 / N)/1000;
        }

    }
    else
        counter--;
}
for(int i = 0; i < 8; i++)
{
    double mag = sqrt(accum[i]*accum[i]+imag[i]*imag[i])/2;
    if(i>3) mag *= -1;
    mags[t*8+i] = (long int) (mag/3);
}

```

Figure 4.13. DFT code

The DFT is handled through this block of code. Inside the for loop, first, the FIFO clock is toggled to get the next data, then the data is read and the real and imaginary parts of the DFT for that sample at the frequency of the transmitted signal are calculated and added to a total. The 15000 and 1000 are used to scale the data to avoid overflows. S is a constant stored in a table used to get the correct frequency for the DFT; it depends on the number of samples and transmitting frequency. Afterwards, the real and imaginary parts are converted to magnitudes.

The set of commands used to control the board via terminal is below. The user can choose between 512, 1024, 2048, 4096, and 8192 samples per channel and between 0.5, 1, 2.5, 5, and 10 kHz transmitting frequencies.

Command	Function
<b>H</b>	Collect homogeneous data
<b>I</b>	Collect inhomogeneous data, run reconstruction, output reconstructed data to GUI
<b>C</b>	Connect GUI serial port to Zedboard
<b>0 – 4</b>	Changes frequency of injected current
<b>5 – 9</b>	Changes number of samples collected from each channel

Table 4.1. Text controls

A GUI also exists for the system, repurposed from a previous project; note that the other controls left on the GUI were from the other project and were not used.

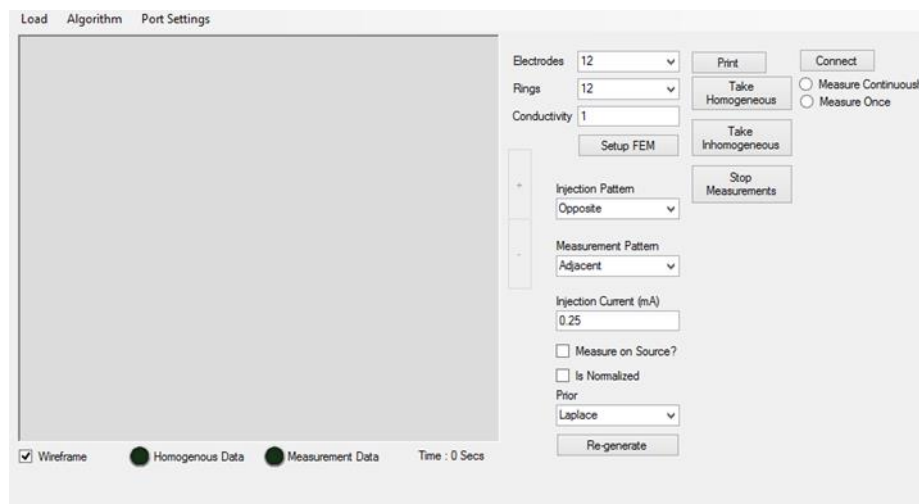


Figure 4.14. GUI screenshot



#### 4.5 Initial Board Results

Here are the results of imaging for a sample round phantom:



Figure 4.15. Phantom image, homogenous data. For inhomogenous data, the left hole was filled and the bottom one was emptied.

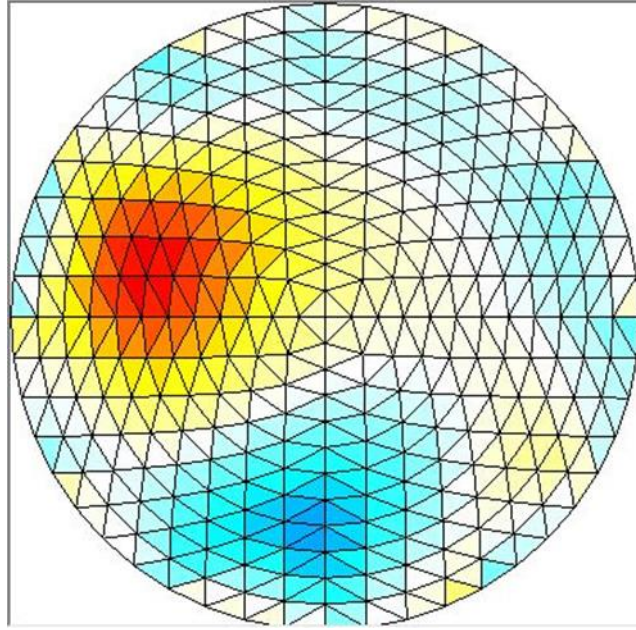


Figure 4.16. Output image, taken with 8192 samples at 10 kHz

Note the triangular construction of the image. The electrodes around the phantom connect to the pins at the left side of the board.

## Chapter 5: Phantom Design

### 5.1 Phantom Overview

The phantom used for this project is made in a 1400 ml recipe which makes a round phantom, which is then cut into the necessary shape for any experiments. The recipe consists of gelatin, distilled water, glycerol, 1-propanol, formaldehyde, and p-toluic acid in the below composition.

<b>Gelatin</b>	167.7 grams
<b>Water</b>	933.8 grams
<b>Glycerol</b>	437.5 grams
<b>1-Propanol</b>	93.4 grams
<b>Formaldehyde</b>	6 grams
<b>p-Toluic Acid</b>	.84 grams
<b>Salt</b>	15 grams

Table 5.1. Phantom composition

### 5.2 Phantom Procedure

Detailed steps of the phantom procedure:

1. Get four beakers: one glass 1L beaker, one glass 2L beaker, and two additional beakers of any size.
2. Measure out 934g of water into the 2L beaker. Add 438g of glycerol.
3. Measure .84g of p-toluic acid into one of the unspecified beakers.
4. Measure out 168g of gelatin into the other unspecified beaker.

5. Put the scale, the hot plate, the mold, the gelatin beaker, the 1L beaker, the 2L beaker, the propanol, the formaldehyde, and the p-toluic acid beaker into the fume hood.
6. Measure out 93g of 1-propanol into the 1L beaker, then add the p-toluic acid.
7. Turn on the hot plate.
8. Put the 1L beaker on the hot plate, then stir until the p-toluic acid is dissolved.
9. Wash out and dry the p-toluic acid beaker.
10. Put the 2L beaker on the hot plate, then add the contents of the 1L and gelatin beakers to it, while stirring. Pour the gelatin in slowly to avoid clumping.
11. Heat the 2L beaker to 75C or until it begins to boil, stirring occasionally.
12. Take the 2L beaker off the hot plate and turn it off.
13. Measure out 6g of formaldehyde into the washed beaker.
14. Wait for the 2L beaker to cool to 50C, then add the formaldehyde and stir.
15. Pour the 2L beaker into the mold.
16. Wait for the phantom to solidify.

## Chapter 6: Proposed Work

### 6.1 Overview

As per the proposal for this project, the proposed work for this thesis was in two parts: First, the development of the EIT system to generate an approximate image for a non-circular phantom without changing the stored Jacobian matrix. This was completed and tested prior to the proposal and was done by adjusting the mesh post-calculation to account for the altered shape.

Second, thorough testing will be done of the system and the results will be documented. This testing will focus on the difference in result quality over varying frequencies and will also use material with a highly frequency-dependent conductivity over the range of frequencies allowed by the system.

This chapter will cover the general outline of how each of these things was done.

### 6.2 Non-circular Phantoms

One goal of the research for this thesis was to produce images with the current system for non-circular phantoms. Due to the way the Jacobian matrix is stored for this system and how it is calculated, the standard techniques involving modifying the Jacobian could not be used; thus, a post-calculation approximation was used to give images of the phantoms. This was done by scaling the output mesh radially to the boundaries of the phantom. This technique successfully generated images of an elliptical and triangular phantom, as well as a circular phantom with the electrodes evenly spaced around a non-central point.

### 6.3 Frequency Dispersion and Cross-frequency Imaging

The other main goal of this thesis was to modify the system to allow for comparing images of different frequencies. This was done by normalizing the output values. While I was unable to find a material with enough frequency dispersion to produce an image without

modifying the phantom between taking the homogeneous and inhomogeneous data, comparison of homogeneous and inhomogeneous data taken at differing frequencies was successful. Testing for this was in two parts: using salt water to show the technique was valid and using a phantom with salt in part of it to attempt to take an image using frequency dispersion alone.

## Chapter 7: Arbitrary Shape Results

### 7.1 Arbitrary Shape Modifications

The design above was modified to allow for different shapes to be used in addition to the circular one. This was done by modifying the GUI to adjust the data for various shapes. The distance from a center point to each electrode relative to the distance from electrode 1 to the center is put in as `electdist`, and all other points in the grid are approximated using a sinc function, and the display is adjusted. This produces an approximation of the image, as shown below.

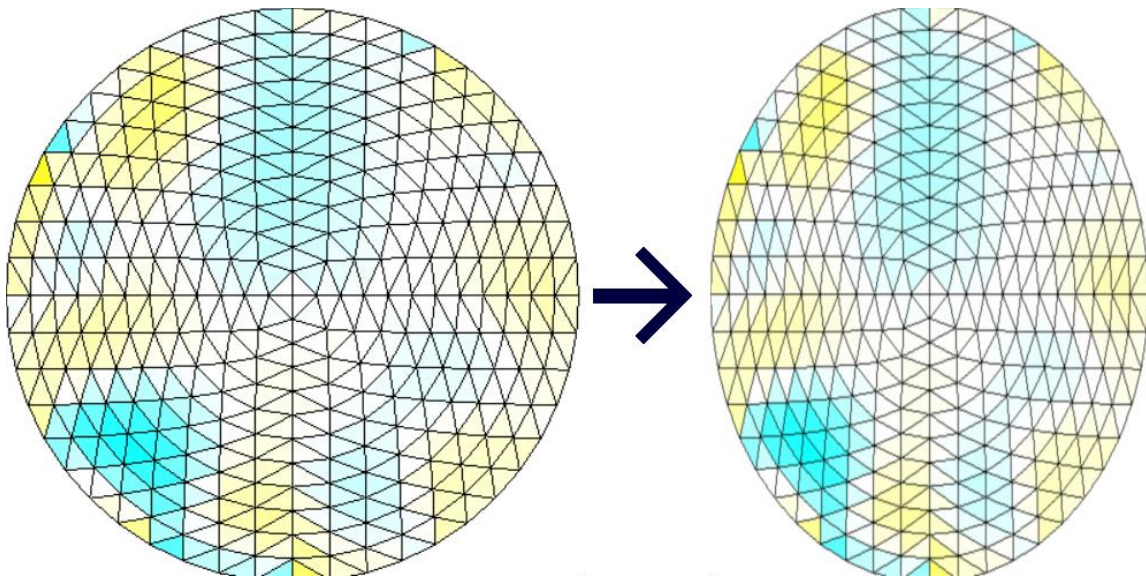


Figure 7.1. A circular mesh and its corresponding elliptical mesh

### 7.2 Arbitrary Shape Algorithm

The relevant block of code is below. The `electdist` in this example is for the off-center circle shown as the third pair of images in Section 7.3. Note that `electdist` must be changed for each shape.

```

for (int j = 0; j < phi.columnNum; j++)
{
//Calculate scaling factor (for non-elliptical testing)
double scalefactor = 0;
phinum = (int)Math.Round(phi[0, j] * 6 / (Math.PI));
double[] electdist = new double[12] {1,.9,.75,.6,.475,.4,.375,.4,.475,.6,.75,.9};
//electdist is the distance from the electrodes (in order) to the center relative to #0.
for (int i = phinum - 120; i <= phinum + 120; i++)
{
double angle = 6 * phi[0, j] - (phinum + i) * Math.PI;
if (angle == 0)
scalefactor += electdist[(phinum + i + 120) % 12];
else
scalefactor += electdist[(phinum + i + 120) % 12] * Math.Sin(angle) / (angle);
}
Location[0, j] = (double)k / rings * Math.Sin((double)phi[0, j]) * scalefactor;
Location[1, j] = (double)k / rings * Math.Cos(phi[0, j]) * scalefactor;
}

```

### 7.3 Arbitrary Shape Results

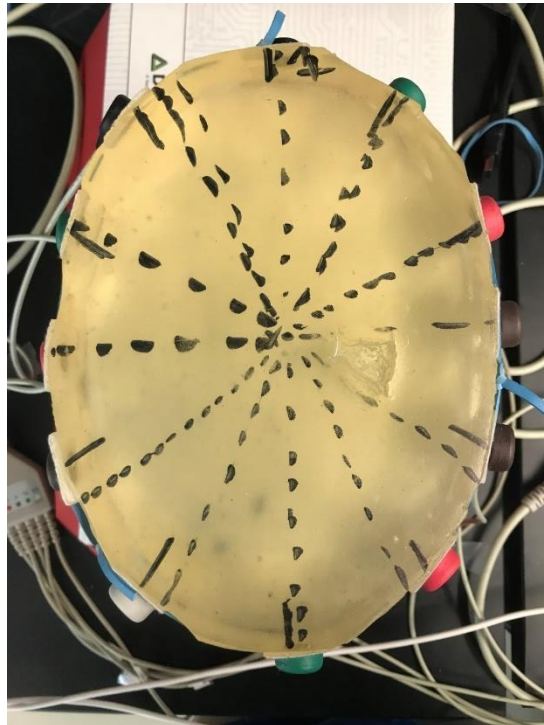


Figure 7.2. Elliptical phantom



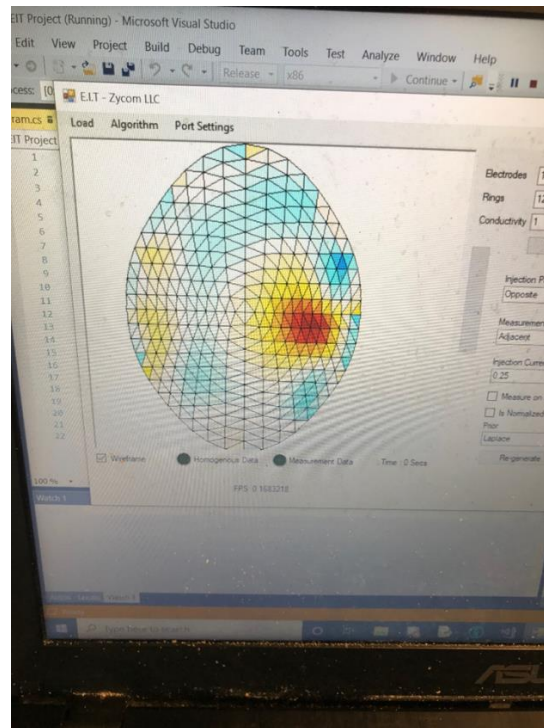


Figure 7.3. Elliptical results

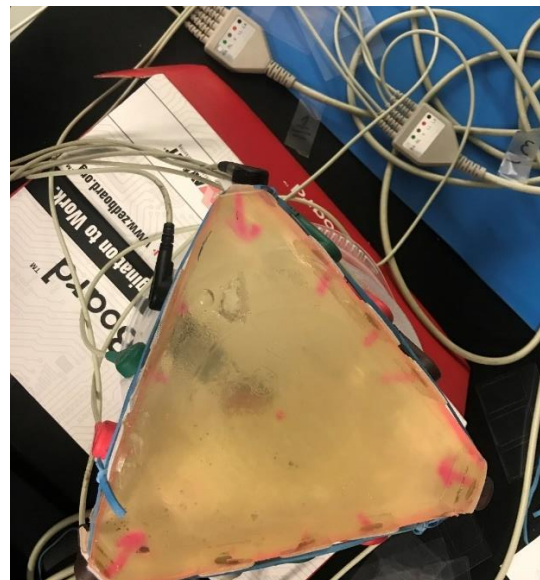


Figure 7.4. Triangular phantom

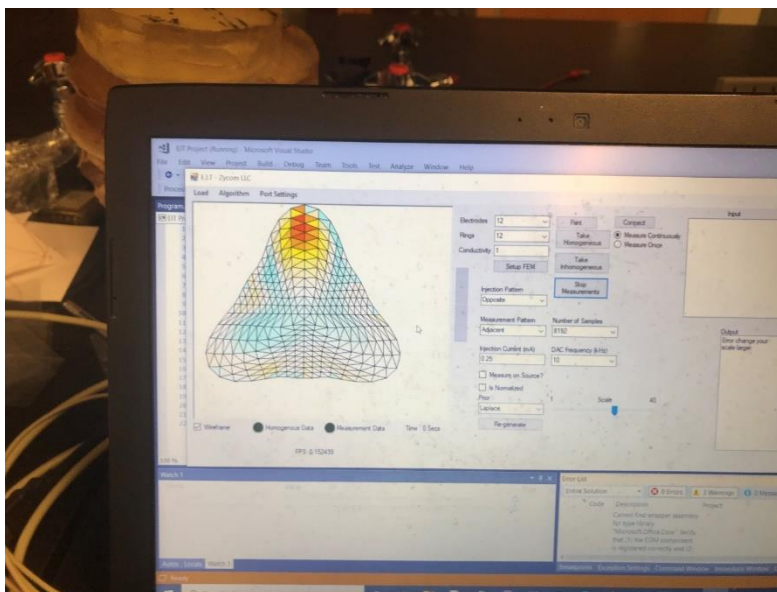


Figure 7.5. Triangular results

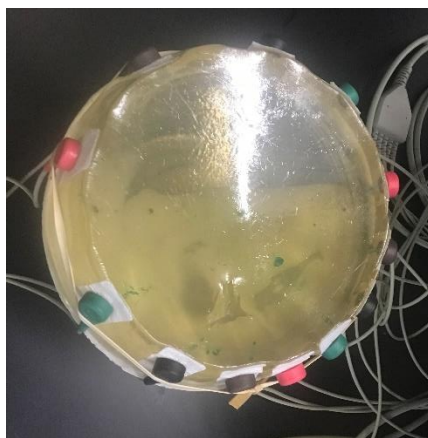


Figure 7.6. Off-center circular phantom. Electrode 1 is the brown one at the top left.

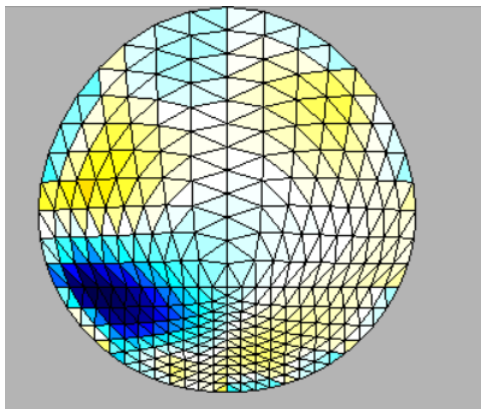


Figure 7.7. Off-center circular image. Image was originally mirrored due to the electrodes being put on counterclockwise, but was corrected.

For the off-center circular phantom, electdist was {1, .9, .75, .6, .475, .4, .375, .4, .475, .6, .75, .9}, as shown above.

## Chapter 8: EIT using Different Frequencies

The EIT reconstruction algorithm traditionally uses the differences between two sets of measurements: a set of data measured with a reference subject (homogeneous), and a second set of data measured with the current subject that is under examination (inhomogeneous). Therefore, EIT is useful to show the changes of tissue conductivities, such as an inserted object in a human body where there are differences between the original measurements and the measurements with the inserted object. Another useful application of EIT is to image changes in tissues over time. However, without a prior reference measurement, the EIT image cannot be formed.

We investigated several methods to form an EIT image without a reference measurement. The first approach we took was to assume that the reference measurements can be produced from a uniform subject. However, the resulting images were not meaningful.

For the second approach, we assumed that tissue is frequency dispersive and that different tissues have different dispersions; thus, the measurements at two different frequencies of two different tissues are not linearly correlated and can be used to form an EIT image to represent the tissue distribution.

We have done numerous experiments using two different frequencies, but they were not successful because the maximum frequency of our EIT system is 10 kHz. We found that there is not much frequency dispersion demonstrated in the lamb brain tissue we used to test the system until above 50 kHz.

Because our current real-time EIT system is limited from a few Hz to 10 kHz, we used the bioimpedance analyzer to manually form an EIT image using 1 kHz and 199 kHz (Sinare; Gegg et al).

In this chapter, three findings are presented:

- 1) Tissue impedance dispersion.
- 2) EIT method using our EIT system with two different frequencies: 500 Hz and 10 kHz with and without salty water, to verify the accuracy of the cross-frequency method.
- 3) EIT method using a bioimpedance analyzer with two different frequencies: 1 kHz and 199 kHz, to study the phantom tissue with lamb brain.

### **8.1 Tissue Impedance Dispersion**

In order to analyze the impedance dispersion of brain tissue, lamb brain tissue was embedded in a phantom, and the impedances from the top to the bottom of the phantom with and without lamb brain were measured using the bioimpedance analyzer and a ZNL3 vector network analyzer.

We found that the impedance with and without the brain tissue are not linearly correlated at high frequencies above 30 kHz using the bioimpedance analyzer.

The study was further investigated and confirmed by using the ZNL3 network analyzer. As shown in Figure 8.1, the transmission coefficients of a phantom without brain embedded were measured from 10 kHz to 5 MHz. Figure 8.2 shows the transmission coefficients of a phantom with brain tissue.

Fig. 8.3 is a graph showing the ratios of transmission coefficients of the phantom and phantom with brain tissue. The chart shows  $(\text{impedance with brain})/(\text{impedance without brain})$ , scaled to the measurement at 5 MHz. It shows no change until 50 kHz, then steadily decreases. This nonlinear curve demonstrates the frequency dispersive properties of the lamb brain tissue.

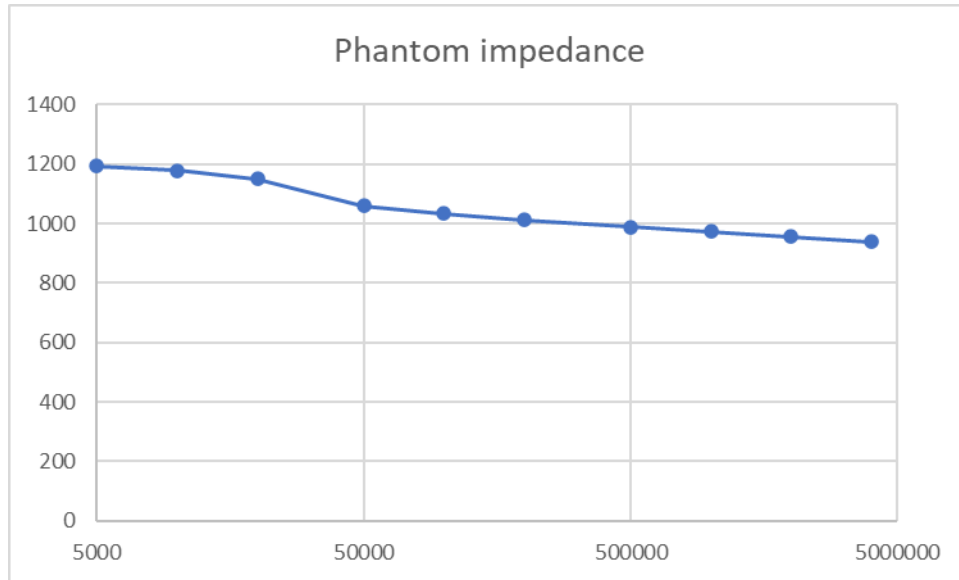


Figure 8.1. Transmission coefficients of tissue phantom

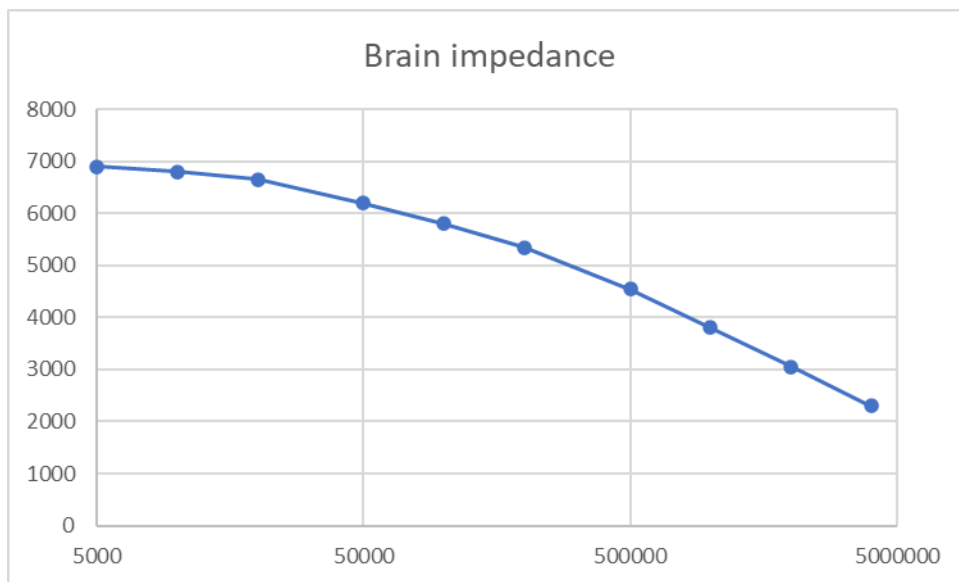


Figure 8.2. Transmission coefficients of tissue phantom with brain tissue

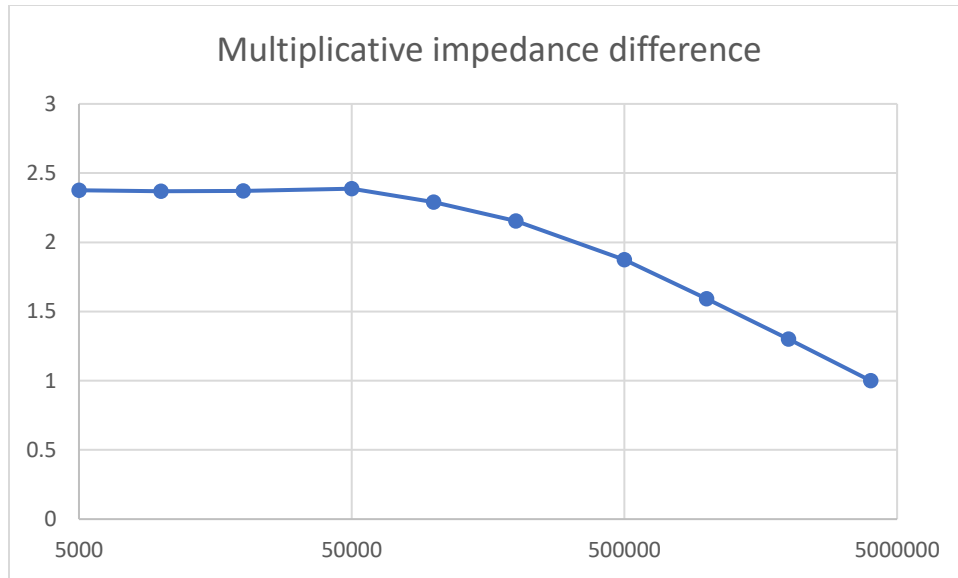


Figure 8.3. Ratios of transmission coefficients of phantom and phantom with lamb brain

## 8.2 EIT Image using Two Different Frequencies for Changed Tissue Phantom

Our realtime EIT system using the ZedBoard was used to take measurements at 500 Hz without salty water and 10 kHz with salty water in a hole. The hole is located at bottom right. The data are individually normalized for the homogeneous and inhomogeneous data before doing the comparison calculation in the EIT algorithm. The normalization is done using equation (8.1).

$$d(k) = \frac{d(k) - \text{mean of } d(k)}{\text{St.D. of all } d(k)} \quad (8.1)$$

```

if (checkBox1_normalize.Checked == true
{
//calculate average
double ave_d1 = d1.Average();
double ave_d2 = d2.Average();
//calculate standard deviation
double d2s = 0;
double d1s = 0;
for (int i = 0; i < 96; i++)
{
d2_new[i] = d2[i] - ave_d2;
d2s += Math.Pow(d2_new[i], 2);
d1_new[i] = d1[i] - ave_d1;
d1s += Math.Pow(d1_new[i], 2);
}
double d1_stdv = Math.Sqrt(d1s / d1.Length);
double d2_stdv = Math.Sqrt(d2s / d2.Length);
//normalize data
for (int i = 0; i < 96; i++)

```

```

{
d1[i] = (d1_new[i] / d1_stdv);
d2[i] = (d2_new[i] / d2_stdv);
}
//compute difference
for (int i = 0; i < 96; i++)
{
diff[i] = d2[i] - d1[i];
}
}

```

This block of code was added to normalize the data. d1 and d2 are the homogeneous and inhomogeneous data sets. The sets are normalized individually, then compared.

While this method was successful at allowing comparisons of different frequency images, no tissue material was found with a resistance dependent enough on frequency to get a meaningful image using the ZedBoard system without modifying the phantom between the homogeneous and inhomogeneous data because the frequency is limited to 10 kHz. This is confirmed by the study described in 8.1, which took place at a later time.

As shown in Figure 8.4, a phantom with a hole (bottom right) was imaged by using two frequencies: 500 Hz and 10 kHz, with and without salty water. The results demonstrate that the method of using two frequencies is working. However, the materials of the phantom are not significantly dispersive in the frequency range from 500 Hz to 10 kHz. Added salty water creates the impedance difference and is correctly presented in the EIT image by using two frequencies.

### **8.3 Differing Frequency Images**

As shown in figures 8.1 to 8.3, the frequency dispersion in lamb brain tissue starts around 50 kHz. Thus, we used the bioimpedance analyzer to obtain EIT data.

The bioimpedance analyzer has a frequency range from 2 Hz to 199 kHz (Gegg et al. ). It provides differential impedance using 4 electrodes. (Zheng et al) A configuration using 8 electrodes was used. For each transmission, 4 measurements were obtained by manually connecting the differential receiver to the two corresponding electrodes at four different



positions. With 8 transmission positions, 32 measurements were obtained at 1 kHz and 32 measurements were obtained at 199 kHz. The differences between the two sets of data were calculated and the EIT image was generated using the code developed by Chen (Chen 1-95).



Figure 8.4. Lamb brain tissue embedded in a tissue phantom

As shown in Figure 8.4, a lamb brain is embedded in tissue phantom. 8 electrodes are uniformly distributed around the phantom. The first electrode is located above the brain tissue. The current of 0.1 mA was transmitted from the top and bottom electrodes (#1 and #5), adjacent differential voltage was measured between #2 and #3 electrodes, #3 and #4 electrodes, #6 and #7 electrodes, and #7 and #8 electrodes. Then the transmission pair is rotated the next position (#2

and #6 electrodes) for 8 rotations. Thus, 32 measurements were obtained at 1 kHz. The procedure is repeated at 199 kHz.

The differences between two sets of data were used to form an EIT image as shown in Figure 8.5.

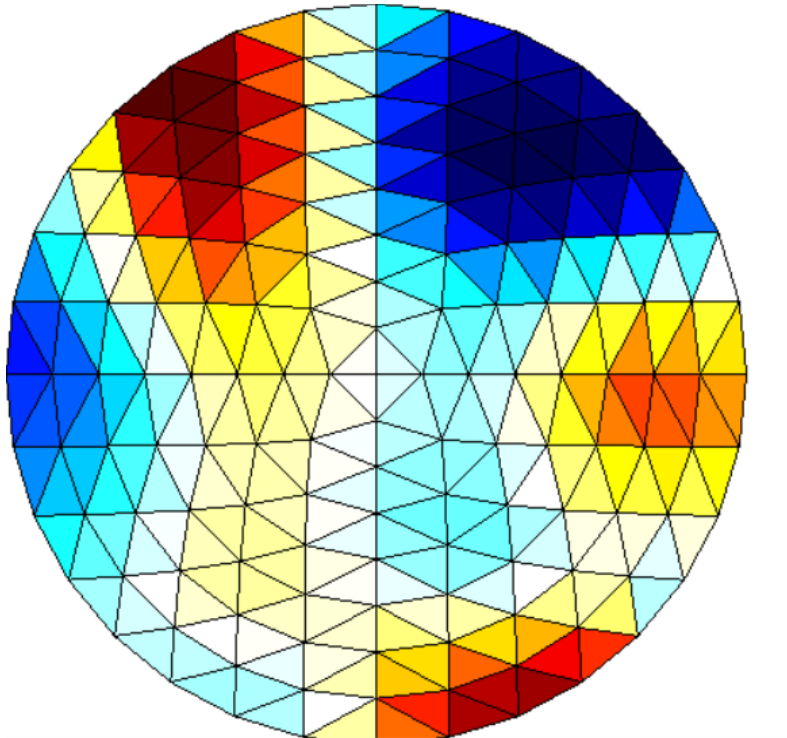


Figure 8.5. EIT image of lamb brain tissue using 500 Hz and 199 kHz.

The lamb brain tissue is located at the top, corresponding to the blue and red area. To prove the correlation of the EIT image and brain tissue, we rotated the phantom by 120 degrees and the resulting EIT image is the same as the rotated image of Figure 8.4.

## Chapter 9: Analysis

### 9.1 Arbitrary Shape Analysis

The normal procedure of the EIT method for imaging a specific shape requires the calculation of a new Jacobian Matrix for the new distribution of the finite elements. This is highly time consuming and may require human intervention.

In this work, a simple and fast EIT imaging method is proposed and verified for arbitrary shapes by simply adjusting the mesh density and distribution in the image domain. As long as the dimensions of the shape are known, the mesh density and distribution will be adjusted accordingly. Thus, the real-time EIT image is formed without changing the basic code or the Jacobian matrix.

The major improvement made here was allowing for non-circular shapes in our real-time EIT system. Because recalculating the Jacobian is a time-consuming process that we can't do while the system is running, this allows for much faster computation of a reasonable image. The method may be limited, however, by somewhat lowered accuracy as the shape of the phantom gets less elliptical.

### 9.2 Multiple Frequency Analysis

Two sets of measurements are required to form an EIT image: homogenous measurements and inhomogeneous measurements. The difference of the two measurements is used to calculate the EIT image. This prevents the study of tissue condition without a priori measurement.

We evaluated the idea of using tissue's frequency dispersive property: the electrical impedance is not linearly correlated at two different frequencies.

Several experiments were performed by using two frequencies: one at 10 kHz and one at a few hundred Hz. No meaningful results were found. The main reason is that the frequency dispersion only starts to show higher than 50 kHz or so, as discovered with later testing.

We showed that the lamb brain tissue has frequency dispersion after 50 kHz. However, our real-time EIT system using the Zedboard is designed to have a maximum output frequency of 10 kHz due to the limited ADC sampling frequency (about 120 kHz). The transmission frequency of our real-time EIT system may be increased to a maximum around 30 kHz, but our study shows that a frequency above 50 kHz is needed.

In the Embedded System Research Lab at St. Cloud State University (SCSU), bio-impedance analyzers have been designed and developed for years. The most recent prototype has a frequency range from 2 Hz to 199 kHz (Gegg et al.). We used this analyzer to manually measure adjacent voltages for an EIT image of 8 electrodes at 500 Hz and 199 kHz. The result image corrected shows the brain tissue location.

The multiple frequency approach is useful for a different kind of imaging than the normal EIT approach; it can image static objects, but only where there is considerable conductivity dispersion in frequency. Our current EIT system cannot take measurements at a wide enough frequency range to use this approach. In order to get good images from it, we would need a system that could have a sampling frequency in MHz, and measure from the hundreds of Hz to 100 kHz or above, whereas the current system can only measure up to 10 kHz.

## **Chapter 10: Conclusion**

A real-time EIT image system was evaluated and studied. The system has 8 channels for the EIT method using 12 electrodes. The measurement frequency ranges from 500 Hz to 10 kHz, or from 1 Hz to 500 Hz using a different analog board. The frame rate is in the order of seconds per frame.

A method to image arbitrarily shaped objects was proposed, implemented, and tested. It effectively completes the EIT calculation and image for elliptical and triangle shapes.

The idea of using EIT to image tissues with frequency dispersion was evaluated. The study found that the lamb brain tissue has frequency dispersive properties when the measurements at 500 Hz and 199 kHz are compared.

### Works Cited

- Burg, et al. “*Real-Time Electrical Impedance Tomography.*” 2018. Senior design report, St. Cloud State University.
- Chen, Xin. *Study on Human brain activity and Electrical Impedance Tomography.* 2012. St. Cloud State University, MSEE.
- Gabriel, et al. “The dielectric properties of biological tissues.” *Physics in Medicine and Biology* vol. 41, no. 11, 1996, pp. 2231-2249.
- Gegg, Nathan, et al. *Bioimpedance Analyzer.* BSEE Senior Design Project. St. Cloud State University. May 2022.
- Polydorides, Nicholas. *Image Reconstruction Algorithms for Soft-Field Tomography.* 2002. Victoria University of Manchester, PhD.
- Sinare, Monali. *Very Low Frequency Electrical Impedance Tomography Image Reconstruction System Using FPGA Software-Hardware Co-design.* 2021. St. Cloud State University, Master of Science in Electrical Engineering. The Repository at St. Cloud State.
- Zheng, Yi, et al. “Screening of Malignant Glioma, Brain Tumors, and Brain Injuries Using Disturbance Coefficient, Differential Impedances, and Artificial Neural Network”. US Patent 11,172,868. 16 Nov 2021.